This article has been accepted for publication in a future issue of this journal, but has not been fully edited. Content may change prior to final publication. Citation information: DOI 10.1109/TIM.2019.2909938, IEEE Transactions on Instrumentation and Measurement

A Moreau Envelope-based Nonlinear Filtering Approach to Denoising Physiological Signals

Priya Ranjan Muduli, *Student Member, IEEE*, and Anirban Mukherjee, *Senior Member, IEEE*

***Abstract*—The recovery of an unknown (or minimally known) physiological signals embedded in noise has been an indispensable topic drawing the attention of many researchers. Restoration of these signals through conventional linear filtering schemes induce over-smoothing effect at jump-discontinuities, and most of the nonlinear filters do not perform well at large noise-level. In this paper, we propose a new nonlinear filtering approach, which incorporates the majorized version of a class of non-smooth functions integrated with Moreau envelope-based regularization. By relaxing the strict sparsifying penalty, the new algorithms balance the smoothness property and the piecewise characteristics of biosignals. We provide the optimality criterion for the proposed algorithms. These algorithms recover the source signals from their noisy measurements. The algorithms outperform the state-of-the-art methods for piecewise synthetic and real-world physiological signals corrupted by additive noise.**

***Index Terms*—Biosignal, Nonlinear Filter, Majorization-minimization, Moreau Envelope, Piecewise Signals.**

I. INTRODUCTION

THE presence of noise in practical measurements is ineluctable. Recovery of vital biosignals from their noisy-measurements is one of the most challenging tasks. Many real-world signals possess sharp discontinuities and are smooth between these transition points. These kinds of signals are known as piecewise signals, and are generated either deliberately, by modulation, or naturally by some typical modeling operations [1], [2]. An exponential polynomial or higher order piecewise polynomial (PP) based approximation model is employed in electrocardiogram (ECG) signals [2], [3]. The blood pressure signal is approximated as PP [4], [5]. Similarly, if the underlying signal has smoothly varying regions separated by many jump-discontinuities, it is known as a piecewise smooth signal (PS). The PS signals may contain multiple bumps and exponential functions. For PS signals, the denoising performance of linear filters is suboptimal owing to the over-smoothing of jump-discontinuities [6]. The splines render a suitable way of modeling 1-D PS functions by allowing for nonuniform knots and different types of building blocks [6]. Applying traditional frequency domain filtering techniques to signals having sharp discontinuities may remove the high-frequency details, and it introduces large, spurious oscillations near the discontinuities, known as Gibb's phenomena [7]. The recovery problem becomes challenging when noise lays over the signal having noticeable sharp discontinuities, which contain high-frequency energy, and are identical to the noisy components. A linear smoother would over-smooth the data; hence, one may contemplate using a nonlinear smoothing algorithm [8]. The wavelet-based denoising methods remove the small-scale detail from the signal, which results in poor time-localization of the remaining large-scale basis functions, and the jumps in the signal cannot be precisely detected. Furthermore, shrinkage induces oscillations near jumps that are not aligned with the jumps in the basis [7]. Measurements resulted from the mixer of additive Gaussian noise, and clean piecewise-signals is one of the most encountered problems. Let us assume that the source signal, $x{=}[x_1, x_2, \cdots, x_N]^T \in \mathbb{R}^N$, is corrupted by an additive noise, $w{\in}\mathbb{R}^N$. The noise w may have certain distribution, such as $\mathcal{N}(0, \sigma_w^2 I_N)$. The corresponding measurement is given by,

$$y = x + w \tag{1}$$

Here, the main objective is to reconstruct $x{\in}\mathbb{R}^N$ from $y{\in}\mathbb{R}^N$. Herein, we predominantly deal with Gaussian noise. The reason why a Gaussian noise makes sense is that practical noise is often the result of summing a large number of different and independent factors, which allows us to apply the central limit theorem.

A. Piecewise Signal Denoising - Prior Art

In the literature on signal reconstruction, there exist numerous algorithms using non-smooth penalty functions, such as total variation (TV) and ℓ_1-norm based filtering techniques [8], [9], [10], [11], [12]. In the context of denoising biosignals, a new recovery framework is proposed to curb the noise-folding effect in practical measurements [13]. A subspace projection-based recovery algorithm is proposed to exploit the hidden structure of biosignals [14]. To remove muscle artifacts from electroencephalogram recordings, a denoising method is proposed by utilizing interchannel dependence information with the combination of multivariate empirical mode decomposition and canonical correlation analysis [15]. A new method for removing motion artifacts from corrupted photoplethysmogram (PPG) signals by applying Fourier series analysis on a cycle-by-cycle basis is presented in [16]. A denoising method is proposed by connecting a Bayesian framework to an ℓ_2-Potts functional for piecewise constant signals [10]. Recently, nonlinear filtering technique using the total variation has emerged as an active topic of research [8], [17]. A hybrid algorithm is proposed by combining both the Tikhonov and total variation regularizations for the reconstruction of signals as a sum of piecewise constant (PC) functions and smooth functions [11]. The total variation-based infimal convolution

The authors are with the Department of Electrical Engineering, Indian Institute of Technology Kharagpur, Kharagpur 721302, India (e-mail: priyaranjan@ee.iitkgp.ac.in; manirban@ieee.org).

This article has been accepted for publication in a future issue of this journal, but has not been fully edited. Content may change prior to final publication. Citation information: DOI 10.1109/TIM.2019.2909938, IEEE Transactions on Instrumentation and Measurement

has shown a potential impact on the recovery of signals from noisy measurements [18]. A model is proposed by combining the total variation semi-norm and ℓ_p-norm for eliminating the staircase effect, a well-known disadvantage of total variation regularization [19]. A more general modified infimal convolution functional is proposed in a discrete setting, which combines ℓ_1-norm with linear operators [20]. In [12], a variation of Hodrick-Prescott filtering called ℓ_1 trend filtering is proposed. It generates linear estimates. Using the Bregman iteration, a split Bregman method is proposed to solve a broad class of ℓ_1-regularized problems and is applied to the RudinOsherFatemi functional for image denoising [21]. A generalized cost function for the estimation of PC signals is proposed with a new penalty function which is characterized by PC signals with light, noisy measurements [17]. In this paper, we propose denoising algorithms which preserve the structure of source signals and recover it from noisy measurements. The new algorithms involve penalty functions with Moreau-envelope and the majorized version of a class of non-smooth functions. We introduce a majorized-logarithm function and a majorized-inverse tangent function using the concept of majorization-minimization (MM) [22] for generating the penalty. Due to the convex relaxation of the strict sparsity-inducing functions, we could enhance the performance of the new algorithms. The majorized-regularizers introduce data-adaptive weights for improving recovery performance. To improve the performance of an optimization algorithm, one may incorporate an initial guess, which is otherwise known as a warm-up step.

The key contributions of this paper are as follows:

- We propose a denoising framework, named as majorized Moreau envelope-based nonlinear filtering (MMNF) for biosignals corrupted by additive noise.
- Two new algorithms are proposed through the MMNF-framework, which employs the majorized logarithmic function and majorized inverse-tangent function, respectively.
- The convexity criterion is derived for the faithful reconstruction of source signals via the proposed MMNF framework. The proposed algorithms outperform the state-of-the-art techniques by reconstructing the biosignals from measurements at various noise levels.

The rest of the paper is organized as follows: Section-II demonstrates the proposed denoising framework. Section-III provides the optimality conditions for the new algorithms. The validation of the proposed algorithms through numerical tests is demonstrated in Section-IV . Finally, the concluding remarks are presented in Section-V.

B. Symbols and Notations

The notations used throughout this paper are provided in Table I.

TABLE I: Symbols and Notations

$\mathbb{R}$	Set of real numbers
$\mathbb{R}^N$	N-dimensional vector space
$\operatorname{argmin} f(\cdot)$	Set of global minimizers of a function $f(\cdot)$
$\Gamma_0(\mathbb{R}^N)$	Lower semi-continuous functions : $\mathbb{R}^N \to]-\infty, +\infty]$
$\lvert x\rvert$	Element-wise absolute operation on $x \in \mathbb{R}^N$
x_i	i^{th} entry of $x \in \mathbb{R}^N$
$\lVert x\rVert_p$	ℓ_p norm of the vector $x \in \mathbb{R}^N$
I_N	Identity matrix of order N
$\mathrm{TV}(x)$	Total Variation operator
D	First-order difference matrix
∇	Gradient operator with respect to x
$(\cdot)^{(l)}$	Values at l^{th} iteration
$\log(\cdot)$	Natural logarithm function

II. PROPOSED DENOISING FRAMEWORK

This section introduces a new denoising technique, which incorporates a class of majorized penalty functions, integrated with infimal convolution (Moreau envelope) in a non-separable optimization framework. The idea of majorization is actuated by the work on majorization-minimization (MM) [22], [23]. The MM is executed in two steps. The first step involves in finding a suitable surrogate function which locally upper bounds the objective-function up to a constant. The second step involves the minimization of the surrogate function. To demonstrate this idea, let us consider a continuous and coercive function, $f{:}\Upsilon \to \mathbb{R}$, i.e., $f(x) \to \infty$ as $\|x\|_2 \to \infty$, where Υ is a non-empty closed convex set in $\mathbb{R}^N$. For all $x \in \Upsilon$, a surrogate function $\mathbb{S}(\cdot|x^{(l)}){:}\Upsilon \to \mathbb{R}$ is generated, such that $\mathbb{S}(x|x^{(l)}) \geq f(x)+c^{(l)}$, where $c^{(l)}=\mathbb{S}(x^{(l)}|x^{(l)})-f(x^{(l)})$. The majorized surface, $\mathbb{S}(x|x^{(l)})$, lies above $f(x)$, and is tangent to it at $x=x^{(l)}$. The sequence $x^{(l)} \in \Upsilon$, $\forall l \in \mathbb{N}$ satisfies the descent property, i.e., $f(x^{(l+1)}) \leq f(x^{(l)})$ [24].

MM steps:

Find a feasible point $x_0 \in \Upsilon$ and set $l = 0$, $\forall\ l \in \mathbb{N}$
repeat
Form $\mathbb{S}(x|x^{(l)})$
$x^{(l+1)} = \arg\min_{x \in \Upsilon} \mathbb{S}(x|x^{(l)})$
$l \leftarrow l + 1$
until convergence

We propose a denoising framework named as Majorized Moreau-envelope based Nonlinear Filtering (MMNF). The concept of MM is used to build the surrogates for the logarithmic-sum and the inverse-tangent functions, and two denoising algorithms, namely MMNF-logsum and MMNF-atan are developed in the MMNF-framework [23]. These denoising algorithms take a noisy measurement, $y \in \mathbb{R}^N$, as input, and produce the estimate of clean source signal , $\hat{x} \in \mathbb{R}^N$, as output. The solution to the MMNF cost function is obtained by the backward-forward splitting (FBS) method [25], which further splits up the main cost function into two separable functionals. These individual functions are processed in the subsequent steps of the FBS-algorithm, which involves an iterative optimization with forward-gradient step and backward estimation step. A schematic of the MMNF framework is presented in Fig. 1.

A. Proposed Method-1

We incorporate a majorized log-sum function integrated with the total variation function to build an upper bound of the $\|Dx\|_1$. Consider a function, $f(x)=f_0(x)+\hat{f}(x)$, with $f_0(x)=\|Dx\|_1$ and $\hat{f}(x)=\log(\epsilon+\|Dx\|_1)$ being a differentiable concave function. Following the idea of linearization

This article has been accepted for publication in a future issue of this journal, but has not been fully edited. Content may change prior to final publication. Citation information: DOI 10.1109/TIM.2019.2909938, IEEE Transactions on Instrumentation and Measurement

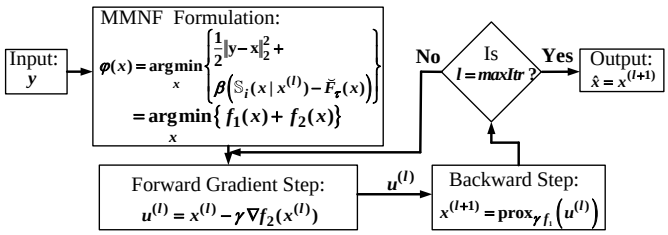

Fig. 1: Schematic of the proposed MMNF framework.

from [22] [23], we propose a new surrogate function of $f(x)$ as

$$\mathbb{S}_{\log}(x|x^{(l)}) = \|Dx\|_1 + \frac{\|Dx\|_1 - \|Dx^{(l)}\|_1}{\|Dx^{(l)}\|_1 + \epsilon} \tag{2}$$

Here $\|Dx\|_1 \leq \mathbb{S}_{\log}(x|x^{(l)})$, and the equality condition holds for $x{=}x^{(l)}$. Since this log-sum majorized function is employed in the proposed MMNF-framework, we name this new algorithm as MMNF-logsum, which is illustrated in Algorithm-1. Here, we define a new penalty function, $\Omega_\tau : \mathbb{R}^N \to \mathbb{R}$ as

$$\begin{aligned}\Omega_\tau(x, x^{(l)}) &= \mathbb{S}_{\log}(x|x^{(l)}) - \breve{F}_\tau(x) \\ &= \|Dx\|_1 + \frac{\|Dx\|_1 - \|Dx^{(l)}\|_1}{\|Dx^{(l)}\|_1 + \epsilon} - \breve{F}_\tau(x)\end{aligned} \tag{3}$$

where $\breve{F}_\tau(x){=}\inf_{z\in\mathbb{R}^N}\left(\|Dz\|_1 + \frac{1}{2\tau}\|x - z\|_2^2\right)$, is the Moreau envelope with $\tau{>}0$ [26]. For $x{\in}\mathbb{R}^N$, it follows the proposition-1 in [17], $\breve{F}_\tau(x) = \|D\ \text{tvd}(x,\tau)\|_1 + \frac{1}{2\tau}\|x - \text{tvd}(x,\tau)\|^2$ and $\nabla\breve{F}(x) = \frac{1}{\tau}\big(x - \text{tvd}(x,\tau)\big),\ \forall\tau > 0$. Here, $\text{tvd}(x,\tau){=}\text{prox}_{\tau\|D\cdot\|_1}(x) = \arg\min_{z\in\mathbb{R}^N}\left\{\frac{1}{2}\|x{-}z\|_2^2 + \tau\|Dz\|_1\right\}$, which is calculated in finite time [9]. The final cost function is formulated by augmenting a quadratic convex fidelity term, $\frac{1}{2}\|y - x\|_2^2$, to the penalty function, defined in (3). The new cost function is

$$\varphi(x, x^{(l)}) \quad = \tfrac{1}{2}\|y - x\|_2^2 + \beta\Omega_\tau(x) \tag{4}$$

Substituting the functional $\Omega_\tau(x, x^{(l)})$ from (3),

$$\varphi(x,x^{(l)}){=}\frac{1}{2}\|y{-}x\|_2^2{+}\beta\Big(\|Dx\|_1{+}\frac{\|Dx\|_1{-}\|Dx^{(l)}\|_1}{\|Dx^{(l)}\|_1{+}\epsilon}{-}\breve{F}_\tau(x)\Big) \tag{5}$$

This problem can be solved by employing the FBS-technique [25]. Let us split the cost function, $\varphi(x, x^{(l)}) : \mathbb{R}^N \to \mathbb{R}$, as

$$\varphi(x, x^{(l)}) = f_1(x) + f_2(x, x^{(l)}) \tag{6}$$

where $f_1(x) = \beta\|Dx\|_1$ and $f_2(x, x^{(l)}){=}\frac{1}{2}\|y - x\|_2^2 - \beta\breve{F}_\tau(x) + \frac{\beta(\|Dx\|_1{-}\|Dx^{(l)}\|_1)}{\|Dx^{(l)}\|_1{+}\epsilon}$.

For the simplicity of operation, we use the iteration index (l) in the FBS steps. Applying the method of FBS to (6), we get the forward step

$$u^{(l)} = x^{(l)} - \gamma\nabla f_2(x^{(l)}) \tag{7}$$

where $\gamma > 0$ and $\nabla f_2(x^{(l)}){=}x^{(l)}{-}y{-}\frac{\beta}{\tau}(x^{(l)}{-}\text{tvd}(x^{(l)},\tau)) + \frac{\beta D^T\text{sign}(Dx)}{\|Dx^{(l)}\|_1{+}\epsilon}$. Here, $\text{sign}(\cdot)$ represents the set-valued signum function, and is defined for $Dx \neq 0$ as: $\text{sign}(Dx){=}\frac{Dx}{|Dx|}$, and for $Dx{=}0$, $\text{sign}(Dx){=}0$. In (7), it should be noted that, the term, $\|Dx^{(l)}\|_1$, is a constant as $x^{(l)}$ represents the value of x at l^{th} iteration. We relax the non-differentiability of ℓ_1-norm by employing its subgradient [27].

The backward updates are obtained by employing the step,

$$\begin{aligned}x^{(l+1)} &= \arg\min_{x\in\mathbb{R}^N}\left\{\tfrac{1}{2}\|u^{(l)}{-}x\|_2^2{+}\gamma f_1(x)\right\} \\ &= \arg\min_{x\in\mathbb{R}^N}\left\{\tfrac{1}{2}\|u^{(l)}{-}x\|_2^2{+}\beta\gamma\|Dx\|_1\right\}\end{aligned} \tag{8}$$

By setting $\gamma{=}1$ [17], we obtain a solution of (8)

$$x^{(l+1)} = \text{tvd}(u^{(l)}, \beta) \tag{9}$$

The final two steps of the proposed algorithm (MMNF-logsum) are as follows:

$$\begin{aligned}u^{(l)} &= y - \frac{\beta D^T\text{sign}(Dx)}{\epsilon + \|Dx^{(l)}\|_1}{+}\frac{\beta}{\tau}(x^{(l)}{-}\text{tvd}(x^{(l)},\tau)) \\ x^{(l+1)} &= \text{tvd}(u^{(l)}, \beta)\end{aligned} \tag{10}$$

Here, the parameter, $\tau{=}\frac{\beta}{\zeta}{>}0$. The smoothing parameter, $\beta{>}0$, and the convexity parameter, $0{<}\zeta{\leq}1$, are suitably chosen to maintain the convexity of the overall cost function. The parameter, $\epsilon > 0$, may be considered as unity.

Algorithm 1 : MMNF-logsum Algorithm

Input: Measurement $y{\in}\mathbb{R}^N$
Output: Estimated source signal, $\hat{x} \in \mathbb{R}^N$

Initialization: smoothing parameter: β, convexity parameter: ζ, Compute $\tau = \frac{\beta}{\zeta}$, max iteration: $maxItr$, $x^{(l)} = 0$.
while $l{\leq}maxItr$ **do**
$u^{(l)} = y - \frac{\beta D^T\text{sign}(Dx)}{\epsilon+\|Dx^{(l)}\|_1}{+}\frac{\beta}{\tau}(x^{(l)}{-}\text{tvd}(x^{(l)},\tau))$
$x^{(l+1)} = \text{tvd}(u^{(l)}, \beta)$
end while
$\hat{x} \leftarrow x^{(l+1)}$
return $\hat{x}$

B. Proposed Method-2

In this method, we incorporate a majorized inverse-tangent function, $\tan^{-1}(\frac{\|Dx\|_1}{\epsilon})$, integrated with the total variation function to build an upper bound of the $\|Dx\|_1$. Let us consider a function, $f(x){=}f_0(x){+}\hat{f}(x)$, with $f_0(x){=}\|Dx\|_1$ and $\hat{f}(x){=}\tan^{-1}(\frac{\|Dx\|_1}{\epsilon})$. The linearization of $\hat{f}(\cdot)$ can be achieved inductively via MM [22] [23], and we introduce a new surrogate function of $f(x)$ as

$$\mathbb{S}_{\text{atan}}(x|x^{(l)}) = \|Dx\|_1 + \frac{\epsilon^2(\|Dx\|_1 - \|Dx^{(l)}\|_1)}{\epsilon^2 + \|Dx^{(l)}\|_1^2} \tag{11}$$

Here $\|Dx\|_1 \leq \mathbb{S}_{\text{atan}}(x|x^{(l)})$. The equality condition holds for $x{=}x^{(l)}$. Since a majorized inverse-tangent function is introduced in the proposed MMNF-framework, we name this new algorithm as MMNF-atan, which is illustrated in Algorithm-2. We define a new penalty function, $\Omega_\tau : \mathbb{R}^N \to \mathbb{R}$ as

$$\begin{aligned}\Omega_\tau(x, x^{(l)}) &= \mathbb{S}_{\text{atan}}(x|x^{(l)}) - \breve{F}_\tau(x) \\ &= \|Dx\|_1 + \frac{\epsilon^2(\|Dx\|_1 - \|Dx^{(l)}\|_1)}{\epsilon^2 + \|Dx^{(l)}\|_1^2} - \breve{F}_\tau(x)\end{aligned} \tag{12}$$

This article has been accepted for publication in a future issue of this journal, but has not been fully edited. Content may change prior to final publication. Citation information: DOI 10.1109/TIM.2019.2909938, IEEE Transactions on Instrumentation and Measurement

The final cost function is formulated by augmenting a quadratic convex fidelity term, $\frac{1}{2}\|y-x\|_2^2$, to the penalty function, defined in (3). The new cost function is

$$\varphi(x,x^{(l)}) \quad = \tfrac{1}{2}\|y-x\|_2^2+\beta\Omega_\tau(x,x^{(l)}) \tag{13}$$

Substituting the functional $\Omega_\tau(x)$ from (12),

$$\varphi=\frac{1}{2}\|y-x\|_2^2+\beta\Big(\|Dx\|_1+\frac{\epsilon^2(\|Dx\|_1-\|Dx^{(l)}\|_1)}{\epsilon^2+\|Dx^{(l)}\|_1^2}-\breve{F}_\tau(x)\Big) \tag{14}$$

The problem can be solved by employing the FBS-technique [25]. Let us split the cost function, $\varphi(x,x^{(l)}):\mathbb{R}^N\to\mathbb{R}$, as

$$\varphi(x,x^{(l)})=f_1(x)+f_2(x) \tag{15}$$

where $f_1(x)=\beta\|Dx\|_1$ and $f_2(x,x^{(l)})=\frac{1}{2}\|y-x\|_2^2-\beta\breve{F}_\tau(x)+\frac{\beta\epsilon^2(\|Dx\|_1-\|Dx^{(l)}\|_1)}{\epsilon^2+\|Dx^{(l)}\|_1^2}$.
For simplicity, we use the iteration index (l) in the FBS steps. Employing the forward gradient step of FBS technique,

$$u^{(l)}=x^{(l)}-\gamma\nabla f_2(x^{(l)}) \tag{16}$$

where $\gamma>0$ and $\nabla f_2(x^{(l)})=x^{(l)}-y-\frac{\beta}{\tau}(x^{(l)}-\text{tvd}(x^{(l)},\tau))+\frac{\beta\epsilon^2D^T\text{sign}(Dx)}{\epsilon^2+\|Dx^{(l)}\|_1^2}$ Here, sign$(\cdot)$ represents the set-valued signum function.
The backward updates are obtained by employing the FBS,

$$\begin{aligned}x^{(l+1)}&=\arg\min_{x\in\mathbb{R}^N}\Big\{\frac{1}{2}\|u^{(l)}-x\|_2^2+\gamma f_1(x)\Big\}\\&=\arg\min_{x\in\mathbb{R}^N}\Big\{\frac{1}{2}\|u^{(l)}-x\|_2^2+\beta\gamma\|Dx\|_1\Big\}\end{aligned} \tag{17}$$

With $\gamma=1$ [17], the problem (17) is solved by the total variation solver [9],

$$x^{(l+1)}=\text{tvd}(u^{(l)},\beta) \tag{18}$$

The final two steps of the proposed algorithm (MMNF-atan) are as follows:

$$\begin{aligned}u^{(l)}&=y+\frac{\beta}{\tau}(x^{(l)}-\text{tvd}(x^{(l)},\tau))-\frac{\beta\epsilon^2D^T\text{sign}(Dx)}{\epsilon^2+\|Dx^{(l)}\|_1^2}\\x^{(l+1)}&=\text{tvd}(u^{(l)},\beta)\end{aligned} \tag{19}$$

The tvd$(\cdot,\cdot)$ can be calculated efficiently by the method [9].

Algorithm 2 : MMNF-atan Algorithm

Input: Measurement $y\in\mathbb{R}^N$
Output: Estimated source signal, $\hat{x}\in\mathbb{R}^N$

Initialization: smoothing parameter: β, convexity parameter: ζ, Compute $\tau=\frac{\beta}{\zeta}$, max iteration: $maxItr$, $x^{(l)}=0$.
while $l\leq maxItr$ **do**
$u^{(l)}=y+\frac{\beta}{\tau}(x^{(l)}-\text{tvd}(x^{(l)},\tau))-\frac{\beta\epsilon^2D^T\text{sign}(Dx)}{\epsilon^2+\|Dx^{(l)}\|_1^2}$
$x^{(l+1)}=\text{tvd}(u^{(l)},\beta)$
end while
$\hat{x}\leftarrow x^{(l+1)}$
return $\hat{x}$

III. OPTIMALITY CRITERION

In this section, we discuss the optimality conditions required for the parameter initialization. Theorem 1 and Theorem 2 provide the convexity condition for the MMNF-logsum and MMNF-atan algorithm, respectively. Both the algorithms follow the same criterion for optimum parameter tuning. The tuning parameters are chosen accordingly by cross-validation to maximize the reconstruction signal-to-noise ratio (RSNR) and to maintain the convexity of the cost functions.

Theorem 1. *Consider the cost function* $\varphi(x,x^{(l)})=\frac{1}{2}\|y-x\|_2^2+\beta\Big(\|Dx\|_1+\frac{\|Dx\|_1-\|Dx^{(l)}\|_1}{\|Dx^{(l)}\|_1+\epsilon}-\breve{F}_\tau(x)\Big)$, *where* $\breve{F}_\tau(x)$ *is the Moreau-envelope, parameterized by* $\tau>0$. *If* $\zeta=\frac{\beta}{\tau}\leq1$, $\beta>0$, *the cost function,* $\varphi(\cdot,\cdot)$, *is convex.*

Proof: We have the cost function defined in (5).

$$\begin{aligned}\varphi(x,x^{(l)})&=\frac{1}{2}\|y-x\|_2^2+\beta\Big(\|Dx\|_1+\frac{\|Dx\|_1-\|Dx^{(l)}\|_1}{\|Dx^{(l)}\|_1+\epsilon}-\breve{F}_\tau(x)\Big)\\&=\frac{1}{2}\|y-x\|_2^2+\beta\Big(\|Dx\|_1+\frac{\|Dx\|_1-\|Dx^{(l)}\|_1}{\|Dx^{(l)}\|_1+\epsilon}\Big)\\&\quad-\beta\min_{z\in\mathbb{R}^N}\Big\{\|Dz\|_1+\frac{1}{2\tau}\|x-z\|_2^2\Big\}\\&=\max_{z\in\mathbb{R}^N}\Big\{\frac{1}{2}\Big(1-\frac{\beta}{\tau}\Big)\|x\|_2^2+\frac{\|y\|_2^2}{2}-x^Ty+\beta\|Dx\|_1\\&\quad+\frac{\beta x^Tz}{\tau}-\frac{\beta\|z\|_2^2}{2\tau}+\beta\Big(\frac{\|Dx\|_1-\|Dx^{(l)}\|_1}{\|Dx^{(l)}\|_1+\epsilon}\Big)\Big\}\\&=\frac{1}{2}\Big(1-\frac{\beta}{\tau}\Big)\|x\|_2^2+\frac{\|y\|_2^2}{2}+\beta\|Dx\|_1+\max_{z\in\mathbb{R}^N}\Big\{\frac{\beta x^Tz}{\tau}\\&\quad+\beta\Big(\frac{\|Dx\|_1-\|Dx^{(l)}\|_1}{\|Dx^{(l)}\|_1+\epsilon}\Big)-\frac{\beta\|z\|_2^2}{2\tau}-x^Ty\Big\}\end{aligned} \tag{20}$$

Since the last term in (20) is affine in x, and is convex, the convexity condition is decided by

$$1-\frac{\beta}{\tau}\geq0\Leftrightarrow\zeta=\frac{\beta}{\tau}\leq1 \tag{21}$$

Here, we define, $0<\zeta=\frac{\beta}{\tau}\leq1$, as the convexity parameter. ■

Theorem 2. *Consider the cost function,* $\varphi(x,x^{(l)})=\frac{1}{2}\|y-x\|_2^2+\beta\Big(\|Dx\|_1+\frac{\epsilon^2(\|Dx\|_1-\|Dx^{(l)}\|_1)}{\epsilon^2+\|Dx^{(l)}\|_1^2}-\breve{F}_\tau(x)\Big)$, *where* $\beta>0$ *and* $\breve{F}_\tau(x)$ *is the Moreau-envelope, parameterized by* $\tau>0$. *The cost* $\varphi(x,x^{(l)})$ *is convex for* $\beta\leq\tau$.

Proof: The proposed algorithms, MMNF-logsum and MMNF-atan, incorporate a similar class of majorized penalty functions. The proof is omitted since the convexity criterion can be derived in a similar way as the proof of Theorem 1. It shows that the cost $\varphi(x,x^{(l)})$ is convex for $\beta\leq\tau$. ■

To set an optimum parameter, $\frac{1}{\tau}$, in the proposed algorithms, we perform several experiments by varying the parameters of the proposed algorithm. In the proposed algorithms, we define the parameter, $\tau=\frac{\beta}{\zeta}$, where $0<\zeta\leq1$ is called the convexity parameter, and $\beta>0$ is the smoothing parameter. We set the parameters, ζ and β, to maximize the RSNR. By employing the MMNF-logsum algorithm on PS and PP measurements, we calculate the corresponding parameters with $\frac{1}{\tau}=0.0021$ and

This article has been accepted for publication in a future issue of this journal, but has not been fully edited. Content may change prior to final publication. Citation information: DOI 10.1109/TIM.2019.2909938, IEEE Transactions on Instrumentation and Measurement

0.018, respectively. Similarly, considering PS and PP measurements for MMNF-atan algorithm, the respective parameters are fixed at $\frac{1}{\tau}$=0.0275 and 0.0188, respectively.

IV. NUMERICAL EXPERIMENTS

We perform various sets of numerical experiments for evaluating the efficiency of the MMNF algorithms. The experiments are conducted in Matlab R2017, running on a system with Intel(R) core(TM) i5-4570 CPU@ 3.2 GHz and 12 GB of RAM. For demonstration purpose, we use the Wavelab [28] to generate various form of synthetic piecewise-structured signals, $x\in\mathbb{R}^N$, with N=1024. The noisy measurements, $y\in\mathbb{R}^N$, with N=1024 are generated by adding noise ($w\in\mathbb{R}^N$) to the clean signal x, i.e., y=x+w. The goal is to estimate x from y. We experiment on measurements with Gaussian noise, $w\sim\mathcal{N}(0,\sigma_w^2 I_N)$, Uniform noise and colored noise. The signal-recovery tests are performed using the first-order difference matrix $D\in\mathbb{R}^{(N-1)\times N}$.

A. Experiment with Synthetic Data

To give more insight regarding the choice of regularizers, we exploit the hidden sparsity structure of PP-source by the first-difference matrix and is shown in Fig. 2. We consider σ_w=$0.1\times$(source amplitude) for generating measurements from noise-free PS and PP signals. For subjective evaluation, the recovery results obtained by the MMNF-logsum and MMNF-atan algorithms on a PP-measurement are depicted in Fig. 3. The PS source signal, the noisy-measurement, and their corresponding recovery results are shown in Fig. 4. Furthermore, we evaluate the performance of state-of-the-art algorithms by varying the noise-level from σ_w=$\eta\times$(source amplitude), where $\eta\in[0.001, 0.35]$. The average root-mean-square-error (RMSE) is used as the performance index. For a given signal $x\in\mathbb{R}^N$, and its estimate $\hat{x}$, RMSE is defined as $\frac{\|x-\hat{x}\|_2}{\sqrt{N}}$. We generate 100 number of independent noisy measurements from a piecewise source signal, and the average-RMSE value is considered. The RMSE performance of the proposed algorithms for a PP-measurement with varying noise-level is depicted in Fig. 5. It justifies the superior recovery performance of these algorithms. The MMNF-logsum algorithm outperforms the MMNF-atan at large noise-levels. The RMSE performance of the proposed algorithms for a PS-measurement with varying the noise-level is depicted in Fig. 6. For PS signals, although the MMNF-logsum algorithm does not perform substantially at low noise levels, it surpasses other algorithms when the noise level is large. This could be due to the heavy penalty assigned to the sparsity-inducing term, $D^T\text{sign}(Dx)$, at low noise region. The new algorithms outperform the state-of-the-art methods, such as ℓ_2 -Potts Model based method [10], ℓ_1-trend filtering [12], split-Bregman anisotropic TV (ATV), the split-Bregman isotropic TV (ITV) [21], iterative clipping TV (IC-TV) [29], isotropic total variation (ISO-TV) [30] and interior-point solver based TV (Int-point.TV) [31] and the universal threshold (Uni-Th) method [32]. This improvement could be due to the relaxation in tight sparsifying penalty functions employed in the proposed algorithms via the MM. The weights assigned to the sparsifying term ($D^T\text{sign}(Dx)$) are signal-adaptive, and are responsible for the success of these algorithms. The convergence of the new algorithms is demonstrated in Fig. 7. The parameters β=0.06 and ζ=0.01 are set for the normalized PP and PS measurements. It is observed that the recovery error ($\|x-\hat{x}\|_2$) reduces with the number of iterations. Furthermore, we study the computational cost of various algorithms concerning their execution time. The computation time for the state-of-the-art methods by varying the signal length (N=2^n, $n\in[4, 14]$) are provided in Table

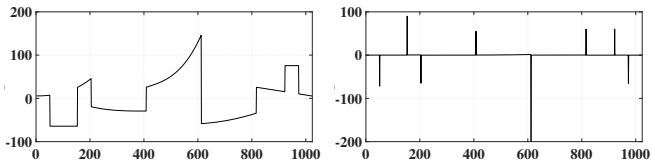

Fig. 2: (a) Noise free PP source, (b) First-difference output.

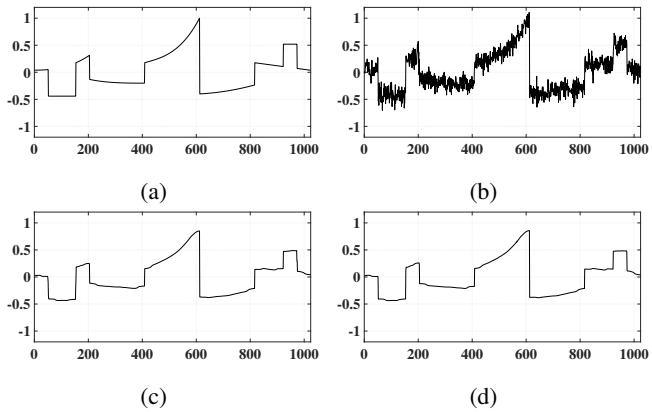

Fig. 3: (a) PP-source signal, (b) PP-measurement (σ_w = $0.1\times$ source amplitude), (c) Denoising using MMNF-logsum (RMSE = 0.0479) and (d) MMNF-atan (RMSE = 0.0309).

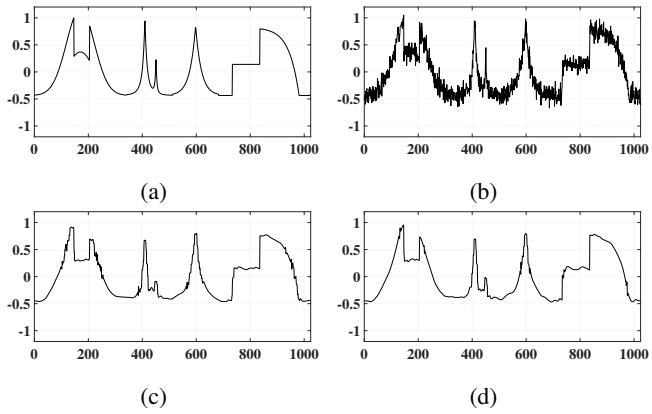

Fig. 4: (a) PS-source signal, (b) PS-measurement (σ_w = $0.1\times$ source amplitude), (c) Denoising using MMNF-logsum (RMSE = 0.0474) and (d) MMNF-atan (RMSE = 0.0408).

This article has been accepted for publication in a future issue of this journal, but has not been fully edited. Content may change prior to final publication. Citation information: DOI 10.1109/TIM.2019.2909938, IEEE Transactions on Instrumentation and Measurement

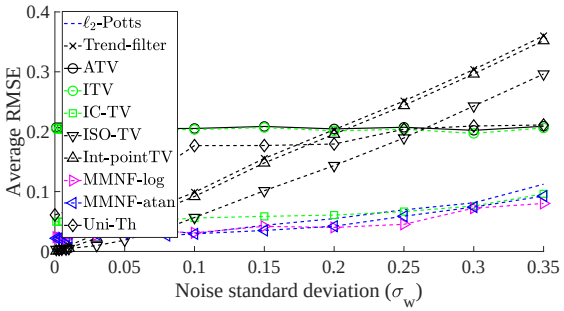

Fig. 5: Average-RMSE vs. noise-level performance for PP-signal.

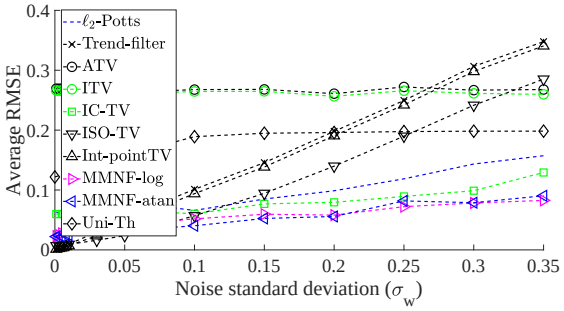

Fig. 6: Average-RMSE vs. noise-level performance for PS-signal.

II. It shows that with increasing the data-length (N), the performance of the proposed algorithms is superior to the prior art except for the IC-TV. The major steps involved in these algorithms are the forward gradient step and the backward update step. The closed form solutions to our cost functions employ the TVD step, which is computed by a fast algorithm [9], with a complexity of $O(N)$ in practical situations, and has the worst case complexity of $O(N^2)$. The forward update step of the proposed algorithm involves a multiplication operation between the banded matrix D (bandwidth=b), and a vector (x). In this case, b=2, i.e., each row of D contains at most 2 non-zero elements with the diagonal elements. This operation costs $2b(N-1)$ flops and gives an overall time-complexity of $O(2bN)$. The operation Dx may be interpreted as the difference of successive entries of x without involving any multiplication operation.

TABLE II: Simulation time (s) with signal length (N=2^n)

Methods	n=4	n=8	n=10	n=12	n=14
[1]ℓ_2-Potts	0.0542	0.6319	7.5072	99.0389	13672
[2]ℓ_2-Potts	0.0656	0.8250	9.5386	107.5634	1266.9
[1]Trend-filter	0.0006	0.0025	0.0074	0.0406	0.2120
[2]Trend-filter	0.0004	0.0041	0.0073	0.0340	0.2202
[1]ATV	0.0057	0.0330	0.0388	0.1181	0.3375
[2]ATV	0.0244	0.0319	0.0492	0.0690	0.2416
[1]ITV	0.0051	0.0356	0.0333	0.1076	0.2967
[2]ITV	0.0141	0.0291	0.0377	0.0537	0.2140
[1]IC-TV	**0.0003**	**0.0004**	**0.0007**	**0.0019**	0.0079
[2]IC-TV	**0.0003**	**0.0004**	**0.0007**	0.0020	**0.0071**
[1]ISO-TV	0.0038	0.0045	0.0080	0.0189	0.0517
[2]ISO-TV	0.0059	0.0053	0.0079	0.0181	0.0485
[1]Int-point.TV	0.0007	0.0018	0.0033	0.0150	0.0791
[2]Int-point.TV	0.0030	0.0029	0.0030	0.0104	0.0558
[1]Uni-Th	0.1753	0.1773	0.1781	0.1789	0.1818
[2]Uni-Th	0.1746	0.1757	0.1785	0.1793	0.1852
[1]MMNF-log	**0.0003**	0.0007	0.0021	0.0152	0.1042
[2]MMNF-log	0.0013	0.0007	0.0022	0.0262	0.1699
[1]MMNF-atan	0.0004	0.0010	0.0031	0.0175	0.1224
[2]MMNF-atan	0.0014	0.0010	0.0031	0.0272	0.1776

[1] for PP signals, [2] for PS signals.

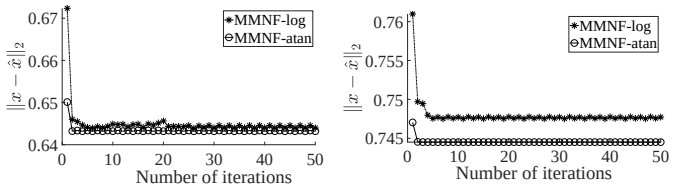

Fig. 7: Recovery error vs. number of iterations for (a) PP measurement and (b) PS measurement.

B. Application to ECG Signals

The structure of real-world ECG signal is exploited via the first difference matrix. We consider a raw ECG sample (Physiobank record: slp02b, sampling rate=250Hz) of 5 seconds from MIT-BIH Polysomnographic database [33]. The Fig. 8 demonstrates the sparsifying nature of total variation-based penalty using a first-order temporal difference. It provides the intuition regarding the choice of the cost function with total variation as its argument. As can be seen, the first difference ECG is sparser than the signal itself. Consequently, for the reconstruction of an ECG, a ℓ_1-norm based algorithm would yield improved performance. The proposed recovery technique employs a majorized Moreau envelope with total variation penalty which preserves the structure of ECG signals. For the reference-based performance evaluation, we generate a noisy measurement y from a source corrupted by noise, $w\sim\mathcal{N}(0,\sigma_w^2)$, and σ_w=$0.1\times$(source amplitude). The recovery results obtained by employing the proposed algorithms are shown in Fig. 9. We set the tuning parameters, $\zeta\in[0.01, 0.1]$ and $\beta \in [10, 20]$ to get maximum RSNR value. We perform a test by varying the noise-level, σ_w=$\eta\times$(source amplitude), where $\eta\in[0.05, 0.3]$. We consider 50 number of raw ECG sources from Physionet database [33]. For each source, 100 number of independent trials are performed, and the average RSNR is considered. Table-III demonstrates the superior recovery performance of the proposed algorithms as compared to the state-of-the-art methods.

This article has been accepted for publication in a future issue of this journal, but has not been fully edited. Content may change prior to final publication. Citation information: DOI 10.1109/TIM.2019.2909938, IEEE Transactions on Instrumentation and Measurement

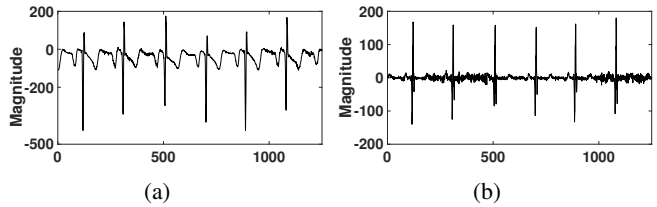

Fig. 8: (a) ECG signal (5 seconds), (b) First-difference ECG.

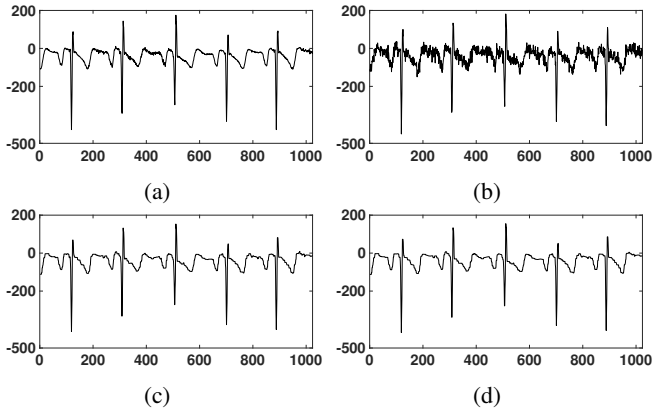

Fig. 9: (a) ECG source (Physiobank: slp02b), (b) measurement, (c) recovery by MMNF-logsum (RSNR $= 21.89$ dB) and (d) MMNF-atan (RSNR $= 22.08$ dB).

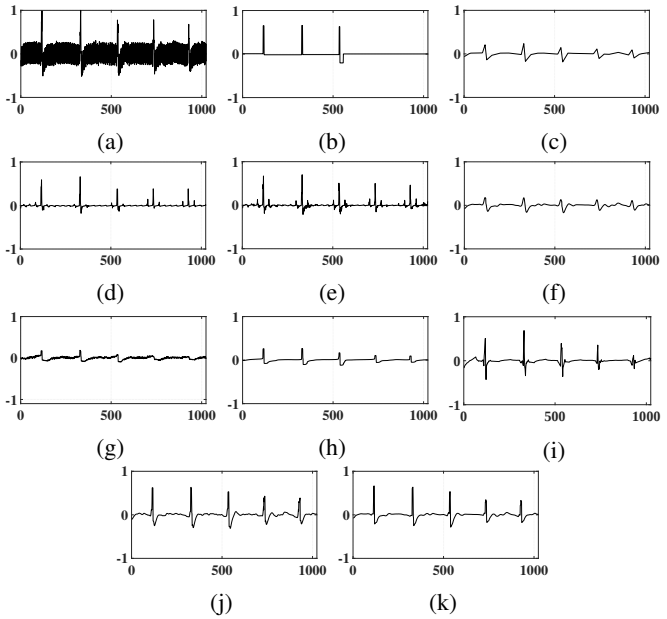

Fig. 10: (a) ECG measurement, (b) recovery by ℓ_2-Potts, (c) Trend-filter, (d) ATV, (e) ITV, (f) IC-TV, (g) ISO-TV, (h) Int-point.TV, (i) Uni-Th, (j) MMNF-logsum and (k) MMNF-atan.

Furthermore, we evaluate the performance of the state-of-the-art algorithms on ECG measurements with implicit noise. We use the noisy-data provided by the Physionet/CinC Challenge-2018 [33], [34]. All the signals are sampled at 200 Hz and are measured in microvolts. We set the parameters, $\beta \in [0.7, 1]$ and $\zeta = 0.9$ by cross-validation. Analysis becomes difficult without the ground truth of the actual signal. Hence, we perform a subjective evaluation of the prior art. The noisy ECG measurements (record:tr03-0005m) and the recovery results obtained by various methods are shown in the Fig 10. Although the state-of-the-art techniques attempt to mimic the shape of a valid source signal, these methods fail to capture the sharp peak of the source. Here, the proposed algorithms seem to have superior performance.

TABLE III: RSNR performance of denoising algorithms for ECG measurements with noise, $\sigma_w = \eta \times$(source amplitude).

Methods	$\eta = 0.05$	$\eta = 0.1$	$\eta = 0.2$	$\eta = 0.3$
ℓ_2-**Potts**	23.43±0.85	18.21±0.98	11.95±0.66	7.41±0.73
Trend-filter	23.42±0.53	18.08±0.72	11.94±0.69	7.42±0.66
ATV	23.41±0.83	18.08±0.66	11.93±0.72	7.41±0.64
ITV	23.42±0.84	18.07±0.56	11.94±0.75	7.42±0.83
IC-TV	24.50±0.63	19.62±0.55	12.74±0.88	7.96±0.74
ISO-TV	23.55±0.76	18.17±0.84	11.98±0.79	7.44±0.65
Int-point.TV	23.64±0.63	18.24±0.75	12.02±0.59	7.45±0.84
Uni-Th	20.09±1.19	17.01±1.05	13.87±1.12	10.15±1.31
MMNF-log	24.62±1.08	22.75±0.99	**17.15±1.21**	**11.42±1.03**
MMNF-atan	**24.69±1.15**	**22.89±1.11**	17.13±1.08	11.40±1.23

C. Application to PPG Signals

Following the PPG-recording set-up of Physionet MIMIC-database, we acquired the raw PPG data (sampled at 125 Hz) from a photoplethysmographic sensor implemented on a customized printed-circuit-board (PCB) of dimension 26×20 mm, as depicted in Fig. 11. We perform the experiments using the bare-PCB with a reflective optical sensor exposed to ambient light. Since the photo-sensor is sensitive to visible light, the noise source could be the variation of ambient light and the base rate of reflected light from the flesh. While acquiring data via the Digilent-Analog-Discovery Kit, we vary

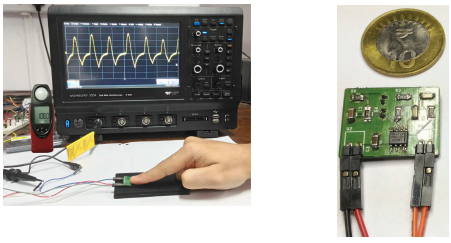

Fig. 11: PPG data acquisition using a customized circuit.

TABLE IV: RSNR performance of denoising algorithms for PPG measurements with noise, $\sigma_w = \eta \times$(source amplitude).

Methods	$\eta = 0.05$	$\eta = 0.1$	$\eta = 0.2$	$\eta = 0.3$
ℓ_2-**Potts**	21.01±0.82	15.11±0.68	8.81±0.58	5.32±0.46
Trend-filter	21.02±0.63	15.12±0.32	8.81±0.49	5.29±0.76
ATV	21.03±0.73	15.12±0.66	8.81±0.87	5.30±0.64
ITV	21.02±0.54	15.11±0.56	8.82±0.65	5.29±0.73
IC-TV	21.23±0.66	15.23±0.45	8.88±0.68	5.34±0.54
ISO-TV	21.03±0.76	15.12±0.54	8.82±0.69	5.31±0.85
Int-point.TV	21.71±0.73	15.50±0.65	9.03±0.59	5.46±0.44
Uni-Th	23.14±1.22	18.31±1.09	11.27±1.01	7.19±0.99
MMNF-log	24.05±1.03	19.27±1.04	**12.46±1.10**	**7.75±1.06**
MMNF-atan	**24.09±1.14**	**19.38±1.00**	12.45±1.18	7.72±1.02

This article has been accepted for publication in a future issue of this journal, but has not been fully edited. Content may change prior to final publication. Citation information: DOI 10.1109/TIM.2019.2909938, IEEE Transactions on Instrumentation and Measurement

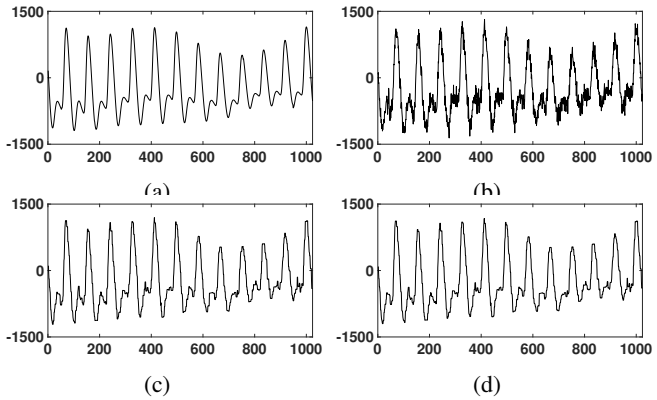

Fig. 12: (a) PPG source, (b) measurement, (c) recovery by MMNF-logsum (RSNR $=$ 19.42 dB) and (d) MMNF-atan (RSNR $=$ 19.49 dB).

the luminance in the range [0-3000] Lux, and the estimated noise-variance due to ambient light ranges from 9.66×10^{-5} to 1.18×10^{-4} ($\approx2.36\times10^{-6}$). For a reference-based evaluation, we add an additional measurement noise, $w\sim\mathcal{N}(0;\sigma_w^2)$, to the raw PPG data. We generate measurement y using the PPG source x, corrupted by noise (σ_w=0.1$\times$source amplitude). The tuning parameters, $\zeta\in[0.01, 0.1]$ and $\beta\in[80, 100]$ are set via cross validation. The recovery results are depicted in Fig. 12. We perform a test by varying the noise-level, $\sigma_w=\eta\times$(source amplitude), where $\eta\in[0.05, 0.3]$. For this test, 20 healthy female and 40 male subjects with age group in $20-45$ years are chosen with their consent. For each subject, 100 number of independent trials are performed, and the average RSNR is considered. Table-IV demonstrates the superior recovery performance of the proposed algorithms.

D. Application to BP Signals

To examine the performance of the proposed algorithms, 50 number of raw blood pressure (BP) data x (sampling rate=250 Hz) from Physiobank [33] are chosen. We perform numerical tests by varying the noise-level, $\sigma_w=\eta\times$(source amplitude), where $\eta\in[0.05, 0.3]$. We set the

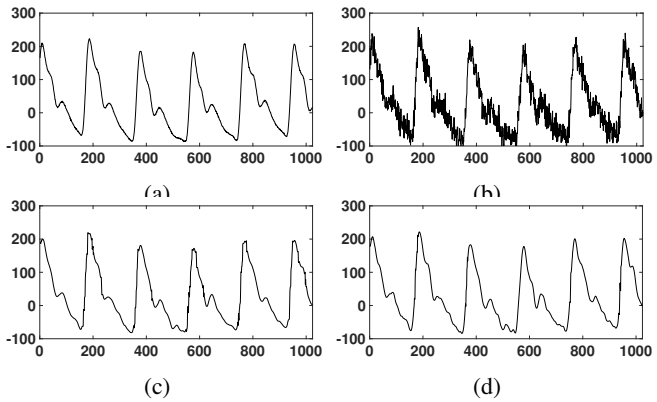

Fig. 13: (a) BP source (Physiobank: slp02b), (b) measurement, (c) recovery by MMNF-logsum (RSNR $=$ 20.56 dB) and (d) MMNF-atan (RSNR $=$ 21.37 dB).

TABLE V: RSNR performance of denoising algorithms for BP measurements with noise, $\sigma_w=\eta\times$(source amplitude).

Methods	$\eta=0.05$	$\eta=0.1$	$\eta=0.2$	$\eta=0.3$
ℓ_2-**Potts**	17.98±0.75	11.77±0.63	5.91±0.78	2.57±0.96
Trend-filter	17.96±0.83	11.78±0.62	5.92±0.79	2.58±0.66
ATV	17.97±0.93	11.79±0.76	5.91±0.67	2.57±0.64
ITV	17.96±0.74	11.78±0.66	5.92±0.85	2.58±0.83
IC-TV	19.16±0.56	12.37±0.75	6.23±0.88	2.78±0.94
ISO-TV	18.01±0.86	11.80±0.64	5.92±0.49	2.58±0.85
Int-point.TV	18.64±0.83	12.10±0.65	6.11±0.89	2.71±0.74
Uni-Th	17.82±1.01	15.58±1.24	14.54±1.01	9.13±1.31
MMNF-log	24.36±1.03	19.19±1.16	**16.09±1.09**	**10.99±1.16**
MMNF-atan	**24.37±1.04**	**19.20±1.12**	16.08±1.08	10.98±1.15

tuning parameters, $\zeta\in[0.1, 0.4]$ and $\beta\in[80, 100]$ to maximize the RSNR value. The Table-V demonstrates the superior recovery performance of the proposed algorithms using the corresponding measurements y. For subjective evaluation of the proposed algorithms, we consider a sample BP source (Physiobank record: slp02b) [33]. The corresponding measurement is obtained by corrupting the source by the noise, $w\sim\mathcal{N}(0, \sigma_w^2)$, and σ_w=0.1$\times$(source amplitude). The recovery results by the proposed algorithms are depicted in Fig. 13.

E. Experiments with Various Types of Noises

In this section, we experiment on various physiological signals using the colored noise (pink/flicker noise) which occurs in all electronics devices [35]. Table-VI demonstrates the superior recovery performance of the proposed algorithms. For visual evaluation, we consider noisy tissue-concentration curve at fractional plasma volumes V_p=0.1, generated by an extended reference region model (ERRM) for dynamic contrast-enhanced magnetic resonance imaging (DCE-MRI) [36]. The noisy measurement contains pink noise, $\sigma_w=0.5\times$ (source amplitude). The recovery results obtained by employing the proposed algorithms are shown in Fig. 14. Furthermore, we evaluate the algorithms on physiological measurements corrupted by Uniform noise, and the respective RSNR values are provided in Table-VII. The performance of the new methods seems more significant in the case of Gaussian noise as compared to the Uniform noise.

TABLE VI: RSNR performance using pink noise.

Methods	ECG	PPG	BP	Tissue conc.
ℓ_2-**Potts**	17.593	21.782	17.729	26.625
Trend-filter	17.594	21.790	17.719	23.684
ATV	17.594	21.791	17.718	23.683
ITV	17.593	21.790	17.719	23.694
IC-TV	18.079	21.887	18.193	26.141
ISO-TV	17.630	21.788	17.739	26.083
Int-point.TV	17.687	21.989	18.032	24.695
Uni-Th	17.394	21.801	17.895	25.595
MMNF-log	18.632	22.780	**19.692**	27.911
MMNF-atan	**18.633**	**22.910**	19.688	**27.919**

This article has been accepted for publication in a future issue of this journal, but has not been fully edited. Content may change prior to final publication. Citation information: DOI 10.1109/TIM.2019.2909938, IEEE Transactions on Instrumentation and Measurement

TABLE VII: RSNR performance of denoising algorithms for physiological measurements with Uniform noise in the interval $(0, b_w)$, $b_w = \eta \times$ (source amplitude).

Methods	$\eta = 0.01$	$\eta = 0.03$	$\eta = 0.1$	$\eta = 0.2$
[1]ℓ_2-Potts	31.59±0.15	22.50±0.29	12.65±0.62	06.51±0.67
[2]ℓ_2-Potts	37.01±0.26	27.46±0.34	17.05±0.45	11.03±0.49
[3]ℓ_2-Potts	33.37±0.22	27.61±0.42	17.81±0.39	11.92±0.72
[4]ℓ_2-Potts	28.49±0.19	26.16±0.33	18.76±0.40	12.93±0.61
[1]Trend-filter	32.34±0.31	22.57±0.41	12.63±0.57	06.50±0.64
[2]Trend-filter	37.09±0.37	27.47±0.25	17.05±0.71	11.03±0.57
[3]Trend-filter	37.88±0.40	28.28±0.61	17.79±0.79	11.91±0.49
[4]Trend-filter	38.35±0.28	28.43±0.54	17.99±0.64	11.83±0.55
[1]ATV	32.35±0.17	22.58±0.47	12.62±0.63	06.51±0.43
[2]ATV	37.40±0.11	27.47±0.39	17.05±0.48	11.04±0.71
[3]ATV	37.88±0.25	28.29±0.61	17.78±0.52	11.92±0.69
[4]ATV	38.34±0.33	28.42±0.40	17.98±0.39	11.82±0.48
[1]ITV	32.37±0.26	22.57±0.51	12.63±0.46	06.52±0.44
[2]ITV	37.42±0.19	27.48±0.35	17.10±0.67	11.04±0.59
[3]ITV	37.89±0.30	28.28±0.49	17.79±0.70	11.91±0.70
[4]ITV	38.35±0.22	28.43±0.55	17.99±0.44	11.83±0.61
[1]IC-TV	29.38±0.27	22.58±0.33	13.01±0.66	06.75±0.48
[2]IC-TV	37.12±0.41	27.53±0.47	17.10±0.39	11.06±0.67
[3]IC-TV	37.42±0.36	28.59±0.51	18.22±0.43	12.19±0.62
[4]IC-TV	38.89±0.18	29.41±0.67	19.11±0.71	12.97±0.73
[1]ISO-TV	32.35±0.29	22.61±0.43	12.66±0.44	06.52±0.66
[2]ISO-TV	37.07±0.16	27.46±0.58	17.05±0.51	11.03±0.43
[3]ISO-TV	37.89±0.24	28.31±0.40	17.81±0.62	11.92±0.59
[4]ISO-TV	38.96±0.34	29.42±0.44	19.10±0.47	12.86±0.61
[1]Int-point.TV	32.30±0.29	22.65±0.72	12.69±0.39	06.54±0.53
[2]Int-point.TV	37.05±0.37	27.60±0.59	17.21±0.48	11.15±0.44
[3]Int-point.TV	37.57±0.19	28.58±0.33	18.08±0.67	12.08±0.67
[4]Int-point.TV	39.00±0.25	29.34±0.45	18.69±0.58	12.27±0.48
[1]Uni-Th	23.26±0.28	21.13±0.35	12.88±0.72	06.89±0.62
[2]Uni-Th	37.04±0.32	27.51±0.44	17.10±0.67	10.97±0.56
[3]Uni-Th	26.51±0.18	24.04±0.61	17.28±0.55	11.89±0.70
[4]Uni-Th	37.60±0.30	29.29±0.47	19.08±0.49	12.92±0.50
[1]MMNF-log	32.40±0.11	23.01±0.45	13.28±0.66	07.29±0.47
[2]MMNF-log	37.46±0.29	27.74±0.63	17.73±0.59	11.72±0.59
[3]MMNF-log	37.90±0.15	28.75±0.49	18.55±0.47	12.79±0.35
[4]MMNF-log	39.09±0.10	**29.42±0.50**	19.12±0.61	**13.01±0.55**
[1]MMNF-atan	**32.40±0.19**	**23.09±0.37**	**13.30±0.40**	**07.31±0.33**
[2]MMNF-atan	**37.48±0.14**	**27.76±0.61**	**17.74±0.55**	**11.73±0.48**
[3]MMNF-atan	**37.91±0.21**	**28.75±0.70**	**18.56±0.29**	**12.81±0.39**
[4]MMNF-atan	**39.10±0.11**	29.42±0.43	**19.13±0.37**	13.01±0.25

Measurement signals: [1]ECG, [2]PPG, [3]BP, [4]Tissue concentration.

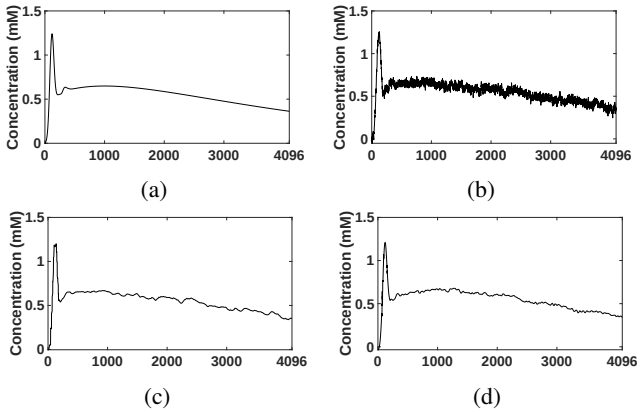

Fig. 14: Tissue concentration (a) source, (b) measurement, (c) recovery by MMNF-log (RSNR=27.91 dB), (d) MMNF-atan (RSNR=27.92 dB).

Remark Although a majority of total variation-based denoising techniques can preserve the sharp discontinuities in case of piecewise constant signals, their performance is suboptimal for piecewise smooth and polynomial measurements. The proposed algorithms balance the smoothness and the sparsifying characteristics of various piecewise signals by introducing the majorized Moreau envelope-based penalty functions. The data-adaptive penalty functions in the framework of MM and FBS enhance the recovery performance of the new algorithms. Although the proposed algorithms have superior recovery performance for measurements with Gaussian noise, their performance is close to other methods for non-Gaussian noises. The parameter β depends on the class of measurement signals and is set by cross-validation. Automated tuning of the parameters employed in the proposed technique may be considered as a future scope of this research work.

V. CONCLUSIONS

In this paper, we propose nonlinear filtering techniques, suitable for denoising physiological signals. The proposed framework (MMNF) introduces penalty functions using the majorized versions of the logarithmic function and inverse-tangent function. These algorithms provide a balance between the smoothness and piecewise constant characteristics of biosignals by relaxing the strict sparsifying penalty. The convexity criterion for the proposed algorithms is derived. Furthermore, the proposed algorithms are robust to recover source signal from measurements at various noise levels.

REFERENCES

[1] J. L. Semmlow and B. Griffel, *Biosignal and Medical Image Processing*. CRC press, 2014.

[2] R. Nygaard and D. Haugland, "Compressing ECG Signals by Piecewise Polynomial Approximation," in *Proc. IEEE Int. Conf. Acoustics, Speech and Signal Processing (ICASSP)*. IEEE, 1998, pp. 1809–1812.

[3] J. S. Arteaga-Falconi, H. A. Osman, and A. E. Saddik, "ECG Authentication for Mobile Devices," *IEEE Trans. Instrum. Meas.*, vol. 65, no. 3, pp. 591 – 600, 2015.

[4] A. Esmaili, M. Kachuee, and M. Shabany, "Nonlinear Cuffless Blood Pressure Estimation of Healthy Subjects Using Pulse Transit Time and Arrival Time," *IEEE Trans. Instrum. Meas.*, vol. 66, no. 12, pp. 3299 – 3308, 2017.

[5] P. J. Aston, M. I. Christie, Y. H. Huang, and M. Nandi, "Beyond HRV: Attractor Reconstruction using the Entire Cardiovascular Waveform Data for Novel Feature Extraction," *Physiological measurement*, vol. 39, no. 2, p. 024001, 2018.

[6] M. Unser and P. D. Tafti, "Stochastic Models for Sparse and Piecewise-smooth Signals," *IEEE Trans. Signal Process.*, vol. 59, no. 3, pp. 989–1006, 2011.

[7] M. A. Little and N. S. Jones, "Generalized Methods and Solvers for Noise Removal from Piecewise Constant Signals. II. New Methods," *Proc Math Phys Eng Sci. / the Royal Society*, vol. 467, no. 2135, pp. 3115–3140, 2011.

[8] L. I. Rudin, S. Osher, and E. Fatemi, "Nonlinear Total Variation based Noise Removal Algorithms," *Physica D: Nonlinear Phenomena*, vol. 60, no. 1-4, pp. 259–268, 1992.

[9] L. Condat, "A Direct Algorithm for 1-D Total Variation Denoising," *IEEE Signal Process. Lett.*, vol. 20, no. 11, pp. 1054–1057, 2013.

[10] J. Frecon, N. Pustelnik, N. Dobigeon, H. Wendt, and P. Abry, "Bayesian Selection for the ℓ_2 -Potts Model Regularization Parameter: 1-D Piecewise Constant Signal Denoising," *IEEE Trans. Signal Process.*, vol. 65, no. 19, pp. 5215–5224, Oct 2017.

[11] A. Gholami and S. M. Hosseini, "A Balanced Combination of Tikhonov and Total variation Regularizations for Reconstruction of Piecewise-smooth Signals," *Signal Process.*, vol. 93, no. 7, pp. 1945–1960, 2013.

[12] S.-J. Kim, K. Koh, S. Boyd, and D. Gorinevsky, "l_1 Trend Filtering," *SIAM review*, vol. 51, no. 2, pp. 339–360, 2009.

[13] P. R. Muduli, A. K. Mandal, and A. Mukherjee, "An Antinoise-Folding Algorithm for the Recovery of Biomedical Signals From Noisy Measurements," *IEEE Trans. Instrum. Meas.*, vol. 66, no. 11, pp. 2909–2916, 2017.

[14] P. R. Muduli and A. Mukherjee, "A Subspace Projection-based Joint Sparse Recovery Method for Structured Biomedical Signals," *IEEE Trans. Instrum. Meas.*, vol. 66, no. 2, pp. 234–242, 2017.

[15] X. Chen, X. Xu, A. Liu, M. J. McKeown, and Z. J. Wang, "The Use of Multivariate EMD and CCA for Denoising Muscle Artifacts from Few-channel EEG Recordings," *IEEE Trans. Instrum. Meas.*, vol. 67, no. 2, pp. 359–370, 2018.

[16] K. A. Reddy, B. George, and V. J. Kumar, "Use of Fourier Series Analysis for Motion Artifact Reduction and Data Compression of Photoplethysmographic Signals," *IEEE Trans. Instrum. Meas.*, vol. 58, no. 5, pp. 1706–1711, 2009.

[17] I. Selesnick, "Total Variation Denoising via the Moreau Envelope," *IEEE Signal Process. Lett.*, vol. 24, no. 2, pp. 216–220, 2017.

[18] A. Chambolle and P.-L. Lions, "Image Recovery via Total Variation Minimization and Related Problems," *Numerische Mathematik*, vol. 76, no. 2, pp. 167–188, 1997.

[19] M. Burger, K. Papafitsoros, E. Papoutsellis, and C.-B. Schönlieb, "Infimal Convolution Regularisation Functionals of BV and [Formula: see text] Spaces: Part I: The Finite Case," *J. Mathematical Imaging and Vision*, vol. 55, pp. 343–369, 2016.

[20] S. Setzer, G. Steidl, and T. Teuber, "Infimal Convolution Regularizations with Discrete l1-type Functionals," *Comm. Math. Sci*, vol. 9, no. 3, pp. 797–872, 2011.

[21] T. Goldstein and S. Osher, "The Split Bregman Method for L1-regularized Problems," *SIAM J. Imaging Sciences*, vol. 2, no. 2, pp. 323–343, 2009.

[22] Y. Sun, P. Babu, and D. P. Palomar, "Majorization-minimization Algorithms in Signal Processing, Communications, and Machine Learning," *IEEE Trans. Signal Process.*, vol. 65, no. 3, pp. 794–816, 2017.

[23] E. J. Candes, M. B. Wakin, and S. P. Boyd, "Enhancing Sparsity by Reweighted l_1 Minimization," *J. Fourier Analysis and Applications*, vol. 14, no. 5-6, pp. 877–905, 2008.

[24] D. R. Hunter and K. Lange, "A Tutorial on MM Algorithms," *The American Statistician*, vol. 58, no. 1, pp. 30–37, 2004.

[25] P. L. Combettes and V. R. Wajs, "Signal Recovery by Proximal Forward-backward Splitting," *Multiscale Modeling & Simulation*, vol. 4, no. 4, pp. 1168–1200, 2005.

[26] H. H. Bauschke and P. L. Combettes, *Convex Analysis and Monotone Operator Theory in Hilbert Spaces*. New York, NY, USA: Springer, 2017, vol. 2011.

[27] J. Duchi and Y. Singer, "Efficient Online and Batch Learning using Forward Backward Splitting," *Journal of Machine Learning Research*, vol. 10, no. Dec, pp. 2899–2934, 2009.

[28] D. Donoho, A. Maleki, and M. Shahram, "Wavelab 850," 2005, accessed 2017-11-01. [Online]. Available: http://statweb.stanford.edu/~wavelab/Wavelab_850

[29] I. W. Selesnick and I. Bayram, "Total Variation Filtering," *White paper*, 2010.

[30] L. Condat, "Discrete Total Variation: New Definition and Minimization," *SIAM J. Imaging Sciences*, vol. 10, no. 3, pp. 1258–1290, 2017.

[31] M. A. Little and N. S. Jones, "Sparse Bayesian Step-filtering for High-throughput Analysis of Molecular Machine Dynamics," in *Proc. IEEE Int. Conf. Acoustics Speech and Signal Process. (ICASSP)*. IEEE, 2010, pp. 4162–4165.

[32] D. L. Donoho and J. M. Johnstone, "Ideal Spatial Adaptation by Wavelet Shrinkage," *Biometrika*, vol. 81, no. 3, pp. 425–455, 1994.

[33] A. L. Goldberger, L. A. Amaral, L. Glass, J. M. Hausdorff, P. C. Ivanov, R. G. Mark, J. E. Mietus, G. B. Moody, C.-K. Peng, and H. E. Stanley, "Physiobank, Physiotoolkit, and Physionet Components of a New Research Resource for Complex Physiologic Signals," *Circulation*, vol. 101, no. 23, pp. e215–e220, 2000.

[34] "Computing in Cardiology (CinC)-2018," accessed 2018-10-01. [Online]. Available: https://physionet.org/physiobank/database/challenge/2018/

[35] N. J. Kasdin, "Discrete Simulation of Colored Noise and Stochastic Processes and 1/f/sup/spl alpha//power law Noise Generation," *Proc. IEEE*, vol. 83, no. 5, pp. 802–827, 1995.

[36] Z. Ahmed and I. R. Levesque, "An Extended Reference Region Model For DCE-MRI that Accounts For Plasma Volume," *NMR in Biomedicine*, vol. 31, no. 7, p. e3924, 2018.

Priya Ranjan Muduli (S'13) received the M.Tech. degree in Electronics and Instrumentation Engineering from the National Institute of Technology Rourkela, Odisha, India in the year 2013. Currently, he is pursuing the Ph.D. degree in the Department of Electrical Engineering, Indian Institute of Technology Kharagpur, Kharagpur, India. His research interests include instrumentation, signal processing, and machine learning.

Anirban Mukherjee (M'07-SM'15) received the M.Tech. and Ph.D. degrees in Electrical Engineering from the Indian Institute of Technology Kharagpur, Kharagpur, India in 2000 and 2005, respectively. From 2004 to 2005, he was with the Tata Consultancy Services Ltd., Kolkata, India. He is currently with the faculty of the Department of Electrical Engineering, Indian Institute of Technology Kharagpur. His principal research interests include signal processing and machine learning.